




# A comparative study of 4-chloro 3-nitro benzophenone crystals grown by slow evaporation solution and Sankaranarayanan–Ramasamy methods

G. Durgababu<sup>1,2,3</sup>, G. Bhagavannarayana<sup>3,\*</sup> , T. Kamalesh<sup>4</sup>, R. Govindaraj<sup>4</sup>, and G. J. Nagaraju<sup>2</sup>

<sup>1</sup>Department of Physics, Rajiv Gandhi University of Knowledge Technologies, Nuzvid, Andhra Pradesh 521202, India

<sup>2</sup>Department of Physics, JNTUK-University College of Engineering, Vizianagaram, Andhra Pradesh 535003, India

<sup>3</sup>VSM Group of Institutions, Ramachandrapuram, E.G. (Dt), Andhra Pradesh 533 255, India

<sup>4</sup>SSN Research Centre, Sri Sivasubramaniya Nadar College of Engineering, Kalavakkam, Tamil Nadu 603110, India

**Received:** 25 January 2022

**Accepted:** 16 February 2022

**Published online:**

10 March 2022

© The Author(s), under exclusive licence to Springer Science+Business Media, LLC, part of Springer Nature 2022

## ABSTRACT

Single crystal of novel organic 4-chloro 3-nitrobenzophenone (4C3N) is grown by both the conventional slow evaporation solution technique (SEST) and Sankaranarayanan–Ramasamy (SR) method from acetone as solvent medium. The grown crystals were subjected to different characterization techniques to unveil the structural, lattice strain, and optical properties. Among these, Powder X-ray diffraction studies of the grown crystals revealed that the crystal system remains same as orthorhombic with few high intense peaks observed at (111), (013), and (213) and lattice strain evaluated in case of SR grown crystals. The high transmittance was observed from UV–Visible spectroscopy studies for SR grown crystals as compared to conventional grown crystals. The cut-off wavelengths were measured at ~ 420 nm, 430 nm and band gap energies at 3.025 eV, 3.052 eV, respectively, for Conventional and SR method grown crystals. The photoluminescent spectra revealed red shift in the emission peaks of grown crystals which are in good coherence with UV–Visible spectra. The crystalline perfection of grown 4C3N crystals were assessed by HRXRD technique. The full width at half maximum values of the diffracted planes (308) confirmed that the crystalline perfection of SR grown crystals is better than that of the crystals grown by SEST method which could be responsible for the enhancement of optical transparency of SR grown crystals.

Address correspondence to E-mail: bhagavanna55@gmail.com

## 1 Introduction

From the past few decades, the researchers were concentrating on the growth of large size good quality crystals for industrial growth of devices for variety of applications. There are two main advantages to grow large size single crystals, the first one is to restrict the number of nucleons while second one is to perfectly align multiple nucleons in the same direction [1]. One more advantage over the above mentioned is the reliability and cost effectiveness. It is one of our continuous interests to grow the large size single crystals for device applications and also to prevent defects with increasing crystal size particularly in case of crystals grown by solution methods. The bulk crystals grown in slow evaporation method may incorporate large number of defects while the crystals grown in Sankaranarayanan-Ramasamy (SR) method [2] possess minimum defects as there is some control on growth parameters like temperature gradient as SR ampoule has long vertical column. The crystal defects, particularly the macroscopic grain boundaries influence the physical properties of the materials as crystals are anisotropic and properties along different crystallographic directions are different. Different growth methods were found to have different influences on both microscopic defects like point defects and their aggregates and macroscopic defects like structural grain boundaries in inorganic crystals. Solvent [3], pH value of solute and solvent [4], and different ambient conditions plays vital role in the single crystal growth of organic and semiorganic compounds. In case of nano-crystals or -materials, size becomes a very crucial role as their properties are size dependent. For example, the paramagnetic properties of cobalt ferrites were enhanced at nano-scale and turns into superparamagnets due to the concentration of base material and temperature [5] as well as precursors [6]. Solvents like acetone and methanol influence to drive and interaction of ZnO nanoparticle growth when compared to water solvent with both thermodynamic and kinetic controls, under the microwave irradiation [7].

As observed in earlier studies, improvement and growth of ceramic nanostructures are possible under controlled conditions using sonochemical [8–10] and hydrothermal synthesis process [11–14] and co-precipitation route [15, 16]. Different unidirectional crystal growth methods have shown great significance to grow high quality crystals [17–20]. In the

recent decades, unidirectional growth of organic/inorganic compounds with economical viability attracted much attention of the researchers and industrialists. One such unidirectional and bulk size crystal growth method is the Sankaranarayanan-Ramasamy (SR) method [21]. Organic compounds grown in SR method such as Benzoglycine revealed the properties like better hardness and relatively defect free single crystals [22], Benzo phenone single crystals for better phase matching applications [23], L-arginine maleate dehydrate single crystals for enhanced mechanical strength [24], ninhydrin single crystals showed a good phase matching angle at  $(30.7 \pm 1)^\circ$  and UV-Vis study showed that the crystal has good transmittance without absorption in the entire visible region of the spectrum [25], hippuric acid single crystals showed segregation of impurities of solvent atoms along the grain boundaries [26] and semiorganic single crystals such as bis(thiourea)zinc(II) chloride single crystals showed fewer defects from dielectric measurements [2], glycine zinc chloride crystals showed high transmittance and less dislocation density [27], sodium acid phthalate single crystals showed good crystalline perfection [28], tetra glycine barium chloride showed less defects from dielectric loss parameters [29], diglycine zinc chloride have less etch pit density with good crystalline perfection [30], bithiourea zinc chloride revealed decrease in dielectric constant and enhancement in micro hardness along growth axis [31], and potassium dihydrogen orthophosphate (KDP) single crystals were grown unidirectionally by SR method. In addition to the above mentioned enhanced properties, SR grown crystals of organic and semi organic single crystals also showed excellent crystalline perfection without grain boundaries or with very low angle grain boundaries, which may not influence the device properties [32]. Pure and doped SR grown KDP and ZTS single crystals [33–35] also showed enhanced optical, nonlinear optical, electrical, and mechanical strength than the same crystals when grown by conventional methods.

Depending on the nature of the material, bulk crystals with required crystalline perfection can be grown conveniently only by certain methods. As mentioned above, SR method is a convenient, cost effective, and simple solution growth method and can be used for the growth of bulk crystals along a desired direction. In the present investigations, single crystals of novel organic 4-chloro 3-nitrobenzophenone

(4C3N) are grown first time by the unidirectional SR method. These crystals are compared with the crystals of same compound grown by conventional slow evaporation solution technique (SEST) for their crystalline perfection and optical properties.

## 2 Experimental

### 2.1 Synthesis and crystal growth

4C3N is an organic compound which dissolves in acetone, ethanol, and methanol. For growth of good size of single crystals, one has to choose a solvent in which the compound dissolves more. Unlike our recent studies on growth and characterization of pure and doped semiorganic [4, 35] and inorganic [34] single crystals, organic single crystals' growth process needs much attention because, these materials are connected by intermolecular weak Vander's-wall interactions and hence have lower melting points or lower sublimation temperatures. But, they have good solubility in many solvents. The titled compound dissolves good amount in acetone. The saturated solution in acetone was prepared at room temperature after purification through recrystallization process. The as prepared saturated solution was kept for controlled evaporation process. 4C3N single crystals were obtained in 30 days with size  $50 \times 10 \times 3 \text{ mm}^3$  using this conventional slow evaporation solution technique (SEST). A typical crystal grown by this method is shown in Fig. 1a.



**Fig. 1** 4C3N single crystals grown in **a** SEST and **b** SR method

As mentioned in the previous section, to grow large size single crystals along a desired direction, unidirectional method of Sankarnarayanan-Ramasamy (SR) method was adopted. In SR method, a small size of seed crystal of 4C3N was placed at the bottom of the SR ampoule in saturated solution with acetone as solvent. The schematic of the ampoule is shown in Fig. 2. In this crystal growth method, the concentration gradient is driven by gravity. The solution at the bottom of the ampoule has more concentration (due to relatively good vertical length of the solution column) compared to that at the top. In this method temperature controllers, ring heaters, and sensors are used to control heating and to have some temperature gradient to have a better concentration gradient. The temperature gradient depends on the thermal properties of the liquid of the reservoir (water is generally used in the reservoir due to its high specific heat). The temperature gradient in the reservoir and the SR ampoule may not be the same. In this method, after a few days we have successfully grown 4C3N crystal as given in Fig. 1b.

### 2.2 Characterization techniques

#### 2.2.1 Powder X-ray diffractometry (PXRD)

The SR grown crystals were crushed into fine powder of homogeneous size with mortar and pestle to record the PXRD spectra. The PXRD pattern was recorded using Bruker Discover D8; Powder X-ray diffractometer using  $\text{CuK}\alpha$  ( $\lambda = 1.5418 \text{ \AA}$ ) radiation. The powder samples were scanned with using  $2\theta$  range of  $10^\circ$  to  $70^\circ$  at a scan rate of  $0.05^\circ$  per minute at

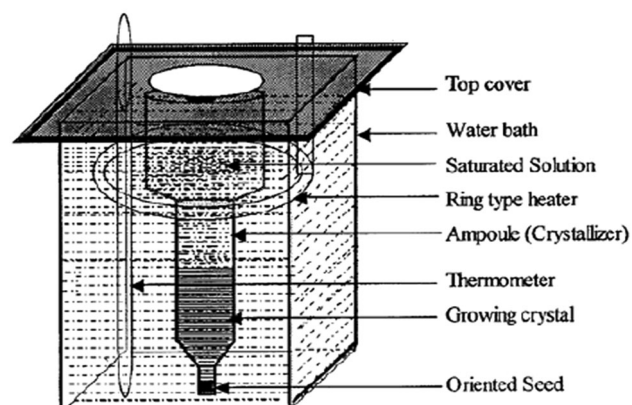


**Fig. 2** SR Growth Setup. Courtesy: N. Balamurugan, M. Lenin, G Bhagavannarayana, P. Ramasamy Cryst. Res. Technol. 42, No. 2, 151–156 (2007)

room temperature (RT). The obtained pattern was well discussed in Sect. 3.1.

### 2.2.2 UV–Visible spectroscopy

The optical transmittance cut-off wavelength and band gap energies of grown crystals were recorded by UV–Visible spectra using CECIL 7400 double beam spectrometer UV–Visible spectrophotometer in the range of 200–900 nm at RT at a scan rate of 200 nm/min with slit width 5 nm. Optical transmission cut-off wavelengths and band gap energies are very much important for device fabrication applications. The conventionally and SR grown crystals were ground and polished with around 1 mm thickness for UV–Visible studies. A diffraction grating of 5 nm slit width was used to get separate visible and UV light beams. In this dual-beam instrument, monochromatic light is split into two beams by a half-mirror device before reaching the sample. One beam is used as a reference. Another beam passes through the sample. The intensity of the reference beam is assumed to be 100% transmitted (or zero absorption) and the value shown by the instrument is the ratio of the intensity of the sample beam to the intensity of the reference beam. The single crystal sample is placed directly into the sample cuvette and the reference cuvette is left empty. The obtained results were well discussed in Sect. 3.2.

### 2.2.3 Photoluminescence (PL) spectroscopy

PL emission spectrum was recorded for grown crystals using Shimadzu, Japan, RF-5301 model spectrometer at RT. The cut-off wavelengths obtained from UV–Visible spectra were chosen for excitation wavelength of the samples grown by both conventional as well as in SR method and scanned in the range of 400–900 nm. The slit widths for both the excitation and emission spectra were fixed at 3 nm. The spectrometer illuminates the fine powder sample with a xenon lamp, which excites the sample, and the intensity of PL emission due to sample relaxation is measured as a function of the wave length. Excitation monochromator isolates a specific wavelength band from xenon lamp light to excite samples placed in the sample holder/sample compartment. Another monochromator known as the emission monochromator selectively accepts the fluorescence emitted by the sample and its photomultiplier tube (PM)

measures the fluorescence intensity. The beam splitter held between the excitation monochromator and the sample is used to measure the intensity of the incident or excited radiation through the PM. The obtained results were discussed in Sect. 3.3.

### 2.2.4 High-resolution X-ray diffractometry

A PANalytical X'Pert PRO MRD high-resolution XRD (HRXRD) system with  $\text{CuK}\alpha_1$  radiation was employed to assess the crystalline perfection of bulk grown crystal specimens whose surface is parallel to the crystallographic planes of (308). The system mainly consists of (i) Fine Focus (0.4mmx12mm) 2 kW X-ray Tube (XRT), (ii) Si(220) four bounce (+, -, -, +) Bartle Monochromator, (iv) Goniometer ( $\pm 0.0001^\circ$ ) for  $\omega$  and  $2\theta$ -rotations, (v) Sample stage with  $\Psi(0.01^\circ)$ ,  $\Phi(0.01^\circ)$  rotations, and X, Y (100 mm) and Z (12 mm) translations and (vii) Scintillation detector.

## 3 Results and discussions

### 3.1 Powder X-ray diffraction (PXRD) studies

To confirm the crystal system and to find the refined lattice parameters, experimentally obtained diffraction data with  $2\theta$  values were used as input to the CHECKCELL refinement software. The obtained lattice constants  $a = 12.9880$  (11) Å,  $b = 7.4451$  (2) Å, and  $c = 24.2981$  (6) Å,  $\alpha = \beta = \gamma = 90^\circ$  and crystalline system remains same as orthorhombic with space group Pbc<sub>a</sub>. The obtained results are in good agreement with the reported values without any change in the angular shift [36]. As seen in Fig. 3a, powder X-ray spectrum of grown crystals, the sharp and high intense peaks were observed at (111), (013), and (213) indicating the high crystalline quality in SR method in comparison to conventionally grown 4C3N crystals [36]. The sharp intense peaks of SR grown 4C3N single crystals may be due to the crystal morphology and its enhanced quality, affected by the diffusion capacity of solvent molecules. [37]. As discussed in our earlier article [34], from Fig. 3a, the relative intensities  $I_{hkl}$  of all possible  $d_{hkl}$  planes, can be used in determining the geometrical or unit cell structure factors ( $F_{hkl}$ ) for the Millar planes as,



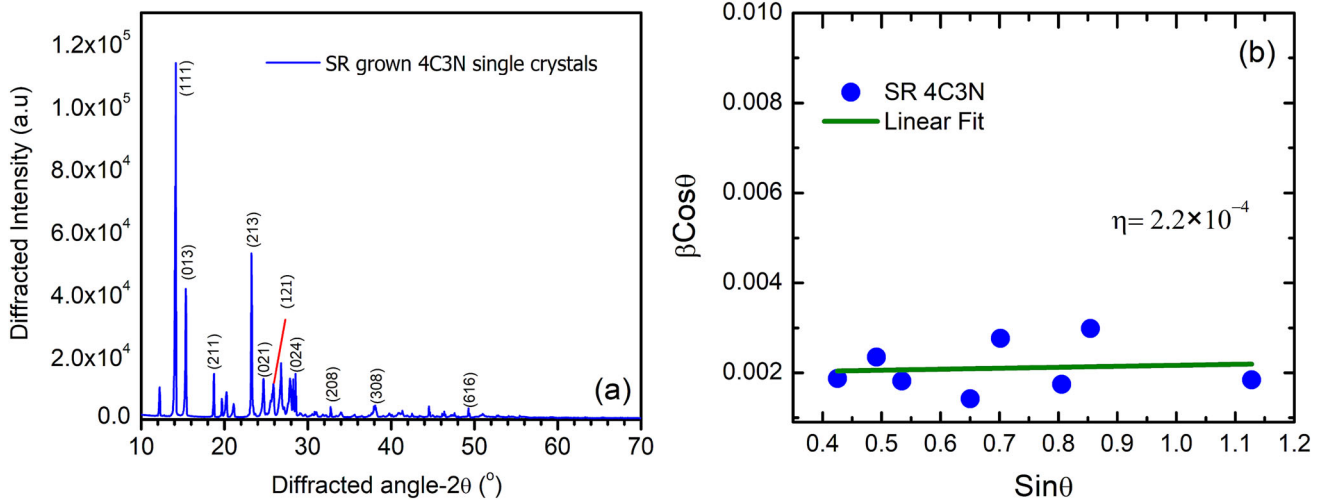


**Fig. 3** Plots of **a** Powder X-ray diffraction spectrum and **b**  $\beta\cos\theta$  vs.  $\sin\theta$  for determination of strain ( $\eta$ ). SR grown 4C3N single crystal

$$I_{hkl} \propto F_{hkl}^2 \tag{1}$$

By comparing the geometrical structure factors (the  $|F_{hkl}|$ 's) obtained from the relative intensities of diffraction peaks of the spectra ( $F_o$ ) and calculated structure factors ( $F_c$ ) for all the theoretically possible crystal structures, one can obtain the crystal structure with lattice parameters. However, the most widely used assessment made by the crystallographers is to know a quantity called the residual factor or *R*-factor, defined as,

$$R = \frac{\sum (||F_o| - |F_c||)}{\sum |F_o|} \tag{2}$$

When the value of *R* is comparatively a small fraction, the proposed structure is treated to be correct and when it is a large fraction, the structure is supposed to be incorrect.

However, the strain in the SR grown single crystals has been evaluated using Williamson Hall relation:

$$\beta \cos \theta = k\lambda/\tau + \eta \sin \theta \tag{3}$$

where,  $\beta$  = full width at half maxima (FWHM) of the diffraction peak in radians,  $\theta$  = Bragg diffraction angle of the peak (half of the peak position on the  $2\theta$ -axis),  $k$  = scherrer constant,  $\lambda$ - wavelength of x-rays,  $\tau$ - crystallite size, and  $\eta$ - lattice strain. The plot drawn between  $\beta\cos\theta$  Vs.  $\sin\theta$  is shown in Fig. 3b. The slope obtained from the linear fit of the data points gives the value of  $\eta$ . The obtained  $\eta$  value from the graph is  $\sim 2.2 \times 10^{-4}$ . The positive value of the slope indicates that the observed defects introduce a slight

compressive strain in the vicinity of defect core [38] and indicates that the defects are of interstitial nature. The low value of strain indicates that the defects are mostly of point defects and their aggregates. The crystallite size ( $\tau$ ) was obtained from the y-intercept ( $k\lambda/\tau$ ) and thus calculated value is  $\sim 1.01 \times 10^{-7}$  m for SR grown single crystals.

### 3.2 UV-visible absorbance studies

The observed transmittance of SR grown crystals is 10% higher than that of conventionally grown 4C3N single crystals in the entire experimental range (Fig. 4a). Due to higher concentration of titled compound driven by the gravity at the bottom of the ampoule, the inclusion of solvents in to the crystalline matrix reduces, which results increase in transmittance in SR grown crystals when compared to crystals grown in SEST method. This improvement in optical transmittance in SR grown crystals may be due to the reduction in scattering centers from crystallographic defects like line defects and structural defects. The decrease in transmittance of conventionally grown crystals may be due to trapping of light by the formation of different defects formed by impurities or inclusion of solvents [39]. The improvement in optical transmittance for the crystals KDP, ADP, TGS, and KAP has been already reported [40].

The cut-off wavelengths of the grown crystals can be obtained from the absorption coefficient ( $\alpha$ ) which is calculated from the transmittance (*T* %) data using Eq. (4). As seen from Fig. 4b, the cut-off wavelengths  $\sim 420$  nm and  $\sim 430$  nm (shown with

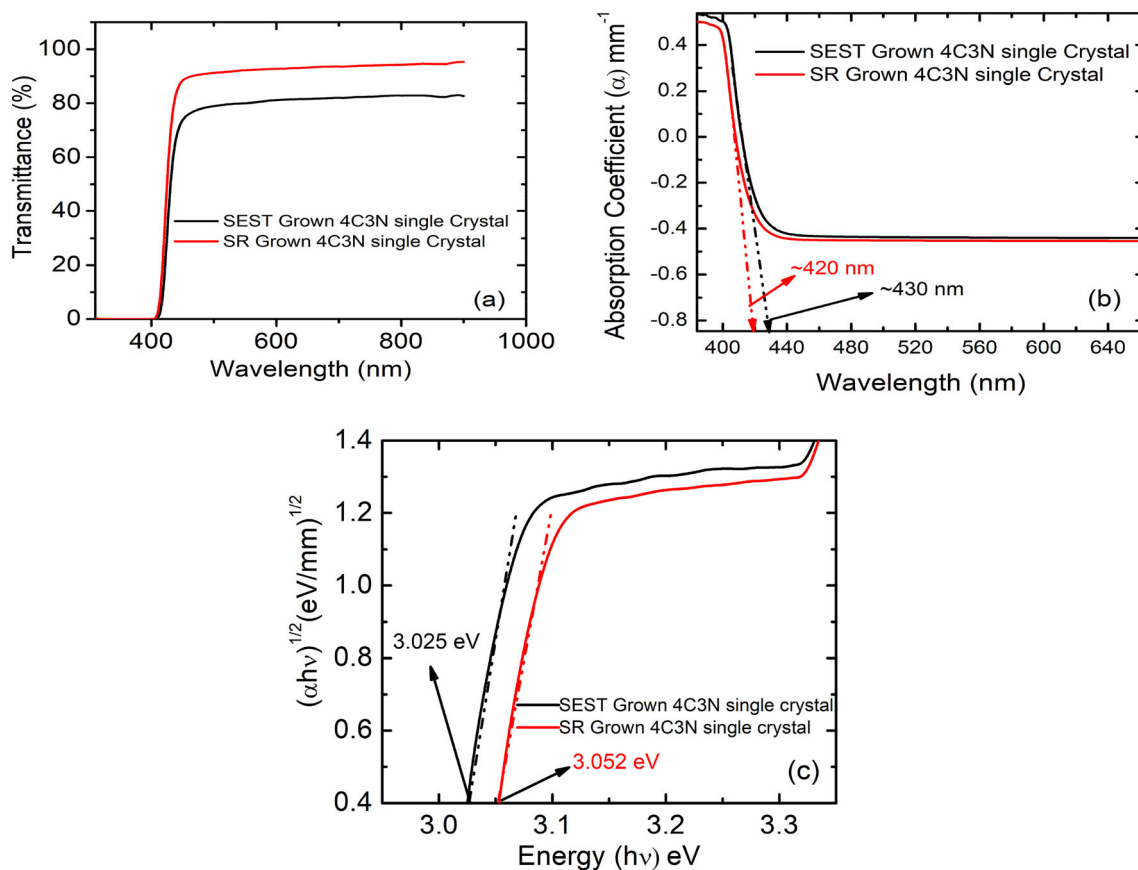


**Fig. 4** UV–Visible **a** transmittance **b** absorbance and **c** band gap energy spectrum of 4C3N single crystals grown in SEST and SR method

dotted lines) were obtained from the plot drawn between absorption coefficient ( $\alpha$ ) and wavelength ( $\lambda$ ) for conventional and SR grown crystals, respectively. The SR grown crystals are very much transparent from 430 to 900 nm wavelength region. The optical band gap energies were calculated from the transmission spectra and absorption coefficient ( $\alpha$ ) near the absorption edge is given by [4],

$$\alpha = \frac{2.303}{t} \log\left(\frac{1}{T}\right) \quad (4)$$

where  $t$ - thickness of the sample and  $T$ - is transmittance of the grown crystals

$$(\alpha hv) = A(hv - E_g)^{1/2} \quad (5)$$

where  $E_g$  is the direct band gap energy,  $A$  is a constant,  $h$ - is plank's constant, and  $\nu$ - is the frequency of light radiation used. The direct band gap energies are estimated from Eq. (5) of plot (c) of Fig. 4, i.e.,  $(\alpha hv)^2$  vs.  $hv$ . The extrapolation of linear portion of the curves of Fig. 4c to the X-axis (shown with dotted lines) gives the band gap energies of the

samples. The obtained band gap energies are 3.025 eV and 3.052 eV for SEST and SR grown crystals respectively. The slight blue shift in band gap energy observed in the grown crystals is good for optical device fabrication applications.

### 3.3 Photoluminescence (PL) studies

Aromatic or multiple conjugate double bonds in organic molecules with high resonance stability is responsible for luminescence behavior of organic compounds [41]. This luminescence property of the compounds finds wide applications in medical, biochemical, and chemistry. In the process of luminescence, when light strikes the sample, part of the light absorbed and the other part gets transmitted, reflected, or scattered. Sample can also emit light after some part of light absorbed in the sample, which is called Photoluminescence. This process of luminescence also depicts the information of defects present in a material without any damage of the material and

hence this technique is known as non-destructive technique (NDT).

The cut-off wavelengths of conventional and SR grown crystals  $\sim 420$  nm and  $\sim 430$  nm, respectively, were chosen for the excitation. The corresponding emission peaks at  $\sim 583$  nm and  $\sim 593$  nm (Fig. 5a, b) were observed in yellow region for the conventional and SR grown crystals, respectively. The emission peaks in the yellow region attributed as the simultaneous existence of vacancy and interstitial defects in the grown crystals which is discussed more in detail in the forth coming analysis of HRXRD in Sect. 3.4 The excitation peaks of grown crystals may be due to the  $n \rightarrow \pi^*$  transition present in the benzophenone group of 4C3N due to the carbonyl (C=O) group [42, 43]. The sharp emission peak's shift was observed in the yellow region of SR grown crystals by  $\sim 10$  nm as compared to the crystals grown in conventional method. This red shift and sharp intensity in PL emission may be due to the slight alteration of electron cloud distribution or mobility of electrons in the ring system in crystals grown by SR method due to better unidirectional growth by electron withdrawing group  $\text{NO}_2$  and electron donating Cl atom. This strong emission peaks observed in both SEST and SR grown organic single crystals are due to very low grain boundaries as discussed in Sect. 3.4. Defects with less density, yield high photoluminescent efficiency as observed in earlier reports [44, 45] much useful for the optoelectronic applications. The high intensity emission peaks observed for the title compound may also be considered for the fabrication of organic light-emitting diodes (OLEDs), organic light-emitting transistors

(OLETs), and even electrically pumped organic lasers.

### 3.4 High-resolution X-ray diffraction (HRXRD) studies

Growth technique and environmental ambient conditions play vital role to grow quality crystals with high crystalline perfection for optical device performance [46, 47]. To accomplish the quality of crystalline perfection of the grown crystals, a high-resolution XRD system (PANalytical X'Pert PRO MRD) with  $\text{CuK}\alpha_1$  radiation is used. The rocking or diffraction curves (DCs) were recorded by performing the so called  $\omega$ -scan with double-axis geometry in symmetrical Bragg geometry. A Four-bounce Si (220) monochromator was used to obtain the  $\text{K}\alpha_1$  beam. A scintillation detector was used to record the diffracted beam from the specimen. No analyzer was used at the receiving stage (i.e., before the detector) to get all the possible information like the individual peaks from structural grain boundaries [48] and scattered intensity from the dislocations and other defects in the specimen crystal.

The grown bulk 4C3N crystal was placed initially in PXRD holder and recorded the diffracted pattern. HRXRD was done on selected ( $hkl$ ) plane, at  $2\theta = 10.5^\circ$  ( $\omega = 4.75^\circ$ ). Further, the obtained  $\text{CuK}\alpha_1$  beam from four bounce silicon (220) bouncer has been collimated by controlling the slits (horizontal/vertical: 0.5 mm/0.25 mm) for present analysis.

Figure 6a shows a DC recorded for SEST grown 4C3N single crystals using (308) diffracting planes. As seen in the figure, the diffraction curve (solid line) is not sharp and the solid curve is a convoluted curve

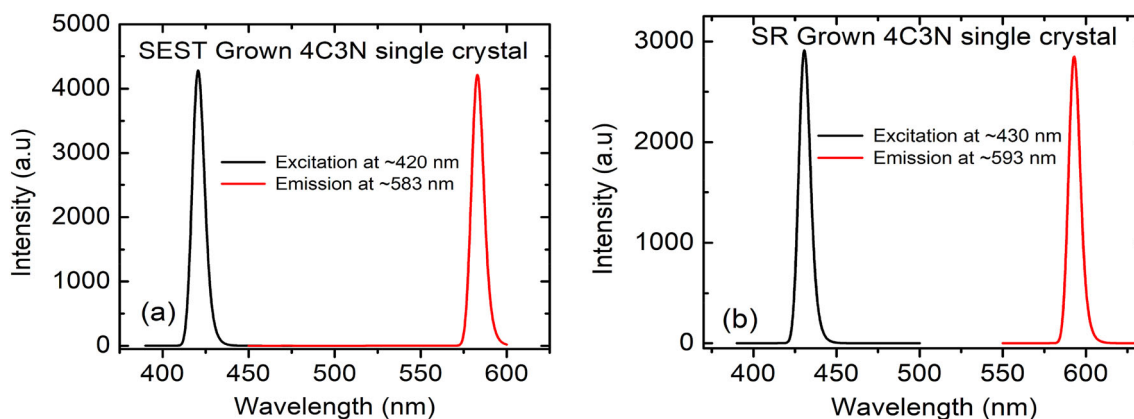


**Fig. 5** Excitation and emission Spectrum of **a** SEST **b** SR grown 4C3N single crystals

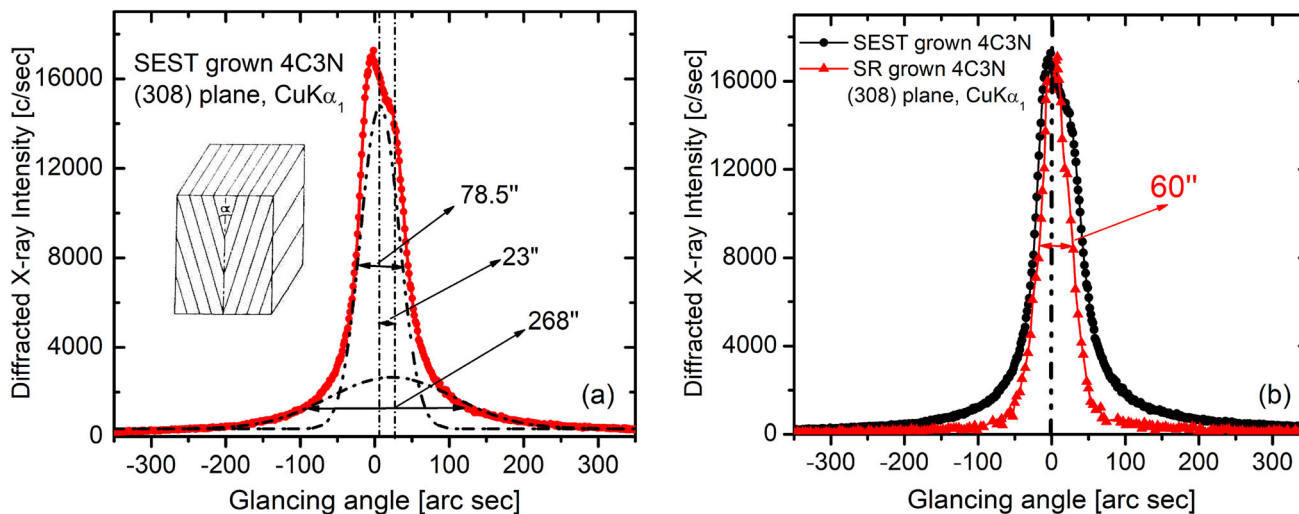


**Fig. 6** Diffraction curves recorded for **a** SEST and **b** SR grown 4C3N single crystals of (308) diffracting planes using  $\text{CuK}\alpha_1$  radiation

of two peaks using the Gaussian fit. This solid curve follows the experimental points (black circles) quite well. The additional peak represents the internal structural grain boundary. The tilt angle, i.e., the misorientation angle ( $\alpha$ ; inset in Fig. 6a) of the boundary with respect to the two adjacent crystalline regions on either sides of the boundary of the observed structural grain boundary is  $\sim 23$  arc s. According to our earlier convention [48], the observed boundary fall under the category of very low angle boundary ( $\alpha \leq 1$  arc min). The very low angle boundary indicates the grown crystal is nearly perfect and quite good. Figure 6b contains the DC recorded for SR grown crystal with full width at half maximum (FWHM) of 60 arc s. For the convenient comparison of DCs of SEST and SR grown specimens, this curve also contains DC of SEST grown crystal. A common range for the glancing angle from  $-300$  to  $+300$  arc s is chosen for the two curves so as to see the relative broadness and asymmetry of the curves with respect to the peak position. As seen from Fig. 6a, the FWHM values of the two peaks corresponding to the two grains of SEST crystal are  $\sim 78.5$  and  $\sim 268$  arc s, which are quite high in comparison with that of SR grown sample, i.e., 60 arc s. These types of defects were also observed in our recently studied SEST grown crystals [4, 34, 35].

The absence of structural grain boundary and the decrease in FWHM of SR grown crystal indicates that the crystalline perfection is enhanced profoundly [49] when compared to 4C3N crystals grown in conventional SEST method. The FWHM of SR grown crystal

in the present study is also quite low in comparison with the same 4C3N crystal grown by Vertical Bridgeman technique [50]. Such kind of unidirectional grown crystals with good crystalline perfection along with high PL intensity as observed in the present investigation are beneficial for high performance optical devices.

## 4 Conclusion

Single crystals of 4C3N were grown successfully by SR techniques for the first time. These SR grown crystals were compared with that of the SEST grown crystals for their crystalline quality and optical properties. The crystal system remains same for SR grown crystals with that of SEST grown crystal as observed by the refined PXRD data with CHECKCELL software. Using the same PXRD data, we could observe the small compressive strain around the defect core of point defects and their aggregates and calculated its quantitative value. The SR grown crystals showed better transmittance over SEST grown crystals in visible and near infrared (NIR) range. The obtained cut-off wavelengths, band gap energies, and emission spectrums are in good coherence with each other. The blue shift was observed from UV-Visible studies in SR grown crystals over the crystals grown by SEST method. The observed blue shift of  $\sim 10$  nm in SR grown crystals in comparison with that of SEST grown crystal indicates the slight alteration or ordering of electron



cloud distribution in the ring system in crystals grown by SR method. Enhanced crystalline perfection with the absence of grain boundaries in case of SR grown crystals as observed by HRXRD technique indicates that the crystals of the title compound can be grown with better quality and bigger size along a desired direction. The relatively good quality SR grown crystals along with high transparency and high PL intensity reveal that the SR grown crystals are good for high performance optical devices like OLEDs, OLETs, organic photo detectors, and photovoltaic devices.

## Acknowledgements

The authors acknowledge Director, Dean Academics of RGUKT-A.P, IIIT, Nuzvid for their support and encouragement. The authors are thankful to the President, Directors and Dr. K. Srinivas Rao, HOD of Physics Department of VSM group of Institutions for their constant encouragement. The authors are highly thankful to Prof. P. Ramasamy for providing instrumentation facilities to characterize the samples at SSN College of engineering, Chennai, Tamil Nadu.

## Author contributions

All authors contributed to the study conception and materials properties. For the material synthesis and design of the experimental work and collection of data and analysis performed by GD, GB, TK, GJN, and RG. The first draft of the manuscript written by GD and authors are read and approved the manuscript.

## Funding

The authors declare that no funds, grants, or other support were received during the preparation of the manuscript.

## Data availability

The data used for analysis part of the manuscript during the current study will be made available by the corresponding author on reasonable request.

## Declarations

**Conflict of interest** The authors have no relevant financial or non-financial interest to disclose.

## References

1. V.L. Nguyen, B.G. Shin, D.L. Duong, S.T. Kim, D. Perello, Y.J. Lim, Q.H. Yuan, F. Ding, H.Y. Jeong, H.S. Shin, S.M. Lee, S.H. Chae, Q.A. Vu, S.H. Lee, Y.H. Lee, *Adv. Mater.* **27**, 1376 (2015)
2. S.K. Kushwaha, N. Vijayan, G. Bhagavannarayana, *Mater. Lett.* **62**, 3931 (2008)
3. C. Sudha, K. Srinivasan, *Cryst. Res. Technol.* **49**, 865 (2014)
4. G. Durgababu, G.J. Nagaraju, G. Bhagavannarayana, *J. Appl. Cryst.* **53**, 972 (2020)
5. O. Karaagac, B. Bilir, H. Kockar, *J. Supercond. Nov. Magn.* **28**, 1021–1027 (2015)
6. F. Ozel, H. Kockar, S. Beyaz, O. Karaagac, T. Tanrisever, *J. Mater. Sci.* **24**, 3073–3080 (2013)
7. P.B. Khoza, M.J. Moloto, L.M. Sikhwivhilu, *J. Nanotechnol.* **2012**, 1687 (2012)
8. S.R. Yousefi, A. Sobhani, H.A. Alshamsi, M. Salavati-Niasari, *RSC Adv.* **11**, 11500–11512 (2021)
9. S.R. Yousefi, O. Amiri, M. Salavati-Niasari, *Ultrason. Sonochem.* **58**, 104619 (2019)
10. P. Mehdizadeh, M. Masjedi-Arani, O. Amiri, A. Al-Nayili, M. Salavati-Niasari, *Fuel* **311**, 122544 (2022)
11. S.R. Yousefi, M. Ghanbari, O. Amiri, Z. Marzhooseyni, P. Mehdizadeh, M. Hajizadeh-Oghaz, M. Salavati-Niasari, *J. Am. Ceram. Soc.* **104**, 2952 (2021)
12. S.R. Yousefi, H.A. Alshamsi, O. Amiri, M. Salavati-Niasari, *J. Mol. Liq.* **337**, 116405 (2021)
13. S.R. Yousefi, M. Masjedi-Arani, M. S. Morassaei, M. Salavati-Niasari, H. Moayedi, *Int. J. Hydrog. Energy.* **44**, 24005 (2019)
14. S.R. Yousefi, D. Ghanbari, M.S. Niasari, *J. Nanostruct.* **6**, 77 (2016)
15. S.R. Yousefi, A. Sobhani, M. Salavati-Niasari, *Adv. Powder Technol.* **28**, 1258 (2017)
16. S.R. Yousefi, D. Ghanbari, M.S. Niasari, M. Hassanpour, *J. Mater. Sci.* **27**, 1244 (2016)
17. K. Lal, G. Bhagavannarayana, *J. Appl. Cryst.* **22**, 209 (1989)
18. G. Bhagavannarayana, S. K. Kushwaha, Mohd. Shakir, K. K. Maurya, *J. Appl. Cryst.* **44**, 122 (2011).
19. A. Choubey, G. Bhagavannarayana, Yu.V. Shubin, B.R. Chakraborty, K. Lal **217**, 515 (2002)
20. Mohd. Shkir, N. Vijayan, Mohd. Nasir, M.A. Wahab, G. Bhagavannarayana, *Optik* **124**, 985 (2013)

21. K. Sankaranarayanan, P. Ramasamy, *J. Cryst. Growth* **280**, 467 (2005)
22. S. Dinakaran, S. Verma, C. Justin Raj, J. Mary Linet, S. Krishnan, S. J. Das, *Cryst. Growth Des.* **9**, 151 (2009).
23. K. Sankaranarayanan, *J. Cryst. Growth* **284**, 203 (2005)
24. U. Charoen-In, P. Ramasamy, P. Manyum, *J. Cryst. Growth* **318**, 745 (2011)
25. N. Rani., N. Vijayan, B. Riscob, S. K. Jat, A. Krishna, S. Das, G. Bhagavannarayana, B. Rathi, M. A. Wahab, *Cryst. Eng. Commun.*, **15**, 2127 (2013).
26. N. Vijayan, G. Bhagavannarayana, M.Z.A. Slawin, *Mater. Lett.* **62**, 2480 (2008)
27. D. Nagaraju, P. V. R. Shekar, T. B. Rao, K. K. Rao, *Mater. Lett.* **64**, 267 (2010).
28. A. Senthil, P. Ramasamy, *J. Cryst. Growth* **311**, 720 (2009)
29. M.S. Pandian, P. Ramasamy, *J. Cryst. Growth* **311**, 944 (2009)
30. M.S. Pandian, P. Ramasamy, *J. Cryst. Growth* **312**, 413 (2010)
31. R. Uthrakumar, C. Vesta, G. Bhagavannarayana, R. Robert, S. J. Das, *J. Alloys Compd.* **509**, 2343 (2011).
32. S. Balamurugan, G. Bhagavannarayana, P. Ramasamy, *Mater. Lett.* **62**, 3963 (2008)
33. S. Balamurugan, P. Ramasamy, *Spectrochim. Acta A* **71**, 1979 (2009)
34. G. Durgababu, G. Swati, N. Vijayan, K.K. Maurya, T. Kamalesh, G.J. Nagaraju, G. Bhagavannarayana, *J. Mater. Sci.* **32**, 5698 (2021)
35. G. Durgababu, G.J. Nagaraju, G. Bhagavannarayana, *J. Mater. Sci.* **32**, 2564 (2021)
36. G.A. Babu, K. Thirupugalmani, P. Ramasamy, K. Ravikumar, *Cryst. Res. Technol.* **44**, 561 (2009)
37. C. Zhang, C. Ji, H. Li, Y. Zhou, J. Xu, R. Xu, J. Li, Y. Luo, *Cryst. Growth Des.* **13**, 282 (2012)
38. G. Bhagavannarayana. PhD thesis, University of Delhi, India, (1994)
39. I.M. Pritula, Yu.N. Velikhov, *Proc. SPIE* **202**, 3793 (1999)
40. M.S. Pandian, N. Balamurugan, V. Ganesh, P.V.R. Shekar, K.K. Rao, P. Ramasamy, *Mater. Lett.* **62**, 3830 (2008)
41. H. H. Willard, L. L. Merritt, J. A. Dean, F. A. Settle, *Instrumental methods of analysis* 7<sup>th</sup> edn. (Belmont Wadsworth, 1988) 513–515.
42. N. Karunakaran, P. Ramasamy, R.P. Ramasamy, *Bull. Mater. Sci.* **37**, 1461 (2014)
43. F. Wilkinson, C.J. Willsher, *Chem. Phys. Lett.* **104**, 272 (1984)
44. R. Katoh, K. Suzuki, A. Furube, M. Kotani, K. Tokumaru, *J. Phys. Chem. C* **113**, 2961 (2009)
45. H. Nakanotani, R. Kabe, M. Yahiro, T. Takenobu, Y. Iwasa, C. Adachi, *Appl. Phys. Express.* **1**, 091801(2008).
46. S.K. Sharma, S. Verma, Y. Singh, K.S. Bartwal, M.K. Tiwari, G.S. Lodha, G. Bhagavannarayana, *Opt. Mater.* **46**, 329 (2015)
47. G. Bhagavannarayana, S. Parthiban, S. Meenakshisundaram, *Cryst. Growth Des.* **8**, 446 (2008)
48. G. Bhagavannarayana, R.V. Ananthamurthy, G.C. Budakoti, B. Kumar, K.S. Bartwal, *J. Appl. Cryst.* **38**, 768 (2005)
49. G. Bhagavannarayana, S. Parthiban, S. Meenakshisundaram, *J. Appl. Cryst.* **39**, 784 (2006)
50. K. Aravinth, G. Anandha Babu, P. Ramasamy, *J. Therm. Anal. Calorim.* **117**, 1165 (2014).

**Publisher's Note** Springer Nature remains neutral with regard to jurisdictional claims in published maps and institutional affiliations.